Investigation on the performances of a twin arm tensioning device

Investigation on the performances of a twin arm tensioning device

Article *in* Proceedings of the Institution of Mechanical Engineers Part D Journal of Automobile Engineering · May 2018
DOI: 10.1177/0954407018775816

5 authors, including:


Maria di Napoli
Politecnico di Torino
2 PUBLICATIONS **1** CITATION
SEE PROFILE


Renato Galluzzi
Politecnico di Torino
14 PUBLICATIONS **19** CITATIONS
SEE PROFILE


Enrico Zenerino
Politecnico di Torino
13 PUBLICATIONS **40** CITATIONS
SEE PROFILE


Andrea Tonoli
Politecnico di Torino
136 PUBLICATIONS **619** CITATIONS
SEE PROFILE

Investigation on the performances of a twin arm tensioning device

Proc IMechE Part D: J Automobile Eng
XX(X):1–10

DOI: 10.1177/ToBeAssigned
www.sagepub.com/
SAGE

Maria di Napoli, Renato Galluzzi, Enrico C Zenerino, Andrea Tonoli and Nicola Amati

Abstract

In the present work, an experimental analysis of the performances of a twin arm tensioner is conducted. The investigated device is used in an automotive belt drive system mounting a belt starter generator. This configuration represents the latest trend of micro-hybrid technologies and is devoted to keep the tension of the belt within a reasonable range, while obtaining the highest possible efficiency in both motor and generator modes. At first, the functionality of a twin arm tensioner is investigated with a static model. Afterwards, the performances of a real tensioner are experimentally assessed through a dedicated test rig in quasi-static conditions. The system is benchmarked in terms of angular displacement of the tensioner arms, belt tensions on the corresponding spans and sliding arc in different operating conditions. Finally, experimental and simulation results are compared. It is shown that the proposed static model is able to capture the behavior of the real device and highlight its functionality.

Keywords

belt drive system, micro-hybrid, hybrid, belt tensioner, belt starter generator, twin arm tensioner, double arm tensioner

Nomenclature

$\hat{}$	accent for peak signal values
bsg	belt starter generator index
cs	crankshaft index
C_i	torque of the ith pulley
F_i	hub load measured on the ith pulley axis
i, u, v	pulley indexes
k	spring stiffness
l_{nom}	nominal length of the belt
l_{ti}	length of the ith belt span
l_{tot}	total length of the belt
$l_{\mathrm{w}i}$	length of the ith wrap
L_i	length of the ith tensioner arm
p	index indicating the nature of the contact point, $p = \mathrm{in}$ for entry or $p = \mathrm{out}$ for exit of the belt on the pulley
R_i	radius of the ith pulley
t	index indicating the belt span type, $t = \mathrm{c}$ for crossed span or $t = \mathrm{d}$ for direct span
T_0	belt pretension at rest
T_i	tension of the ith belt span
x_i, y_i	Cartesian coordinates of the ith pulley center
x_{0i}, y_{0i}	Cartesian coordinates of the ith pulley center at rest
α_i	wrap angle on the the ith pulley
β_{tj}	angle between the horizontal and the belt span itself
γ_i	angle between the ith lever arm and the applied force
δ	pulley rib angle
$\Delta\theta_0$	angular aperture of the twin arm tensioner at rest
θ_i	angular position of the ith pulley
μ	static friction coefficient of the pulley contact
μ_{r}	equivalent friction coefficient for the V-ribbed pulley
ξ_i	angle between the horizontal and the line connecting the centers of the ith and $(i+1)$th pulleys
ϕ_{s}	sliding arc on the BSG pulley

1 Introduction

In traditional vehicles, the belt drive system is in charge of distributing part of the power produced by the engine to the accessories, which are connected to the crankshaft by means of a belt. Speed and torque losses inevitably hamper the performance of a belt drive system (BDS). They affect the transmission efficiency and induce vibrations and noise.

Department of Mechanical and Aerospace Engineering, Politecnico di Torino, Italy

Corresponding author:
Renato Galluzzi, Department of Mechanical and Aerospace Engineering, Politecnico di Torino, Corso Duca degli Abruzzi 24, Turin, Italy
Email: renato.galluzzi@polito.it

The phenomenology of such losses has been intensively studied in the past 50 years by many authors. Literature presents a consolidated classification of the speed losses into four major contributions:[1] belt creep, radial compliance, shear deflection and seating and unseating. In this context, Gerbert provided a first analytical formulation for flat belts and then extended it to V and V-ribbed belts.[2]

The characteristics of modern V-ribbed belts allow to attribute most of the speed losses due to belt-pulley contact to the circumferential shear acting on the rubber layer between the tension layer and the pulley.[3] By converse, torque losses depend on the hysteresis of the belt during its wrapping motion around the pulleys of the BDS. Three main loss sources were identified, i.e. bending, longitudinal loading and radial compression of the belt.[4] These losses have been experimentally investigated in several research activities.[5,6]

The research has developed several technological solutions to overcome the critical issues that characterize BDSs. Belts, pulleys and belt tensioners have faced progressive modifications over the years to optimize the different components that define the rotational and longitudinal motions taking place into the front end accessory drive.

At present, the automotive field employs V-ribbed belts predominantly. Such belts offer a compromise between the features of their predecessors, namely flat and V belts. They guarantee flexibility and high power capacity.[7] In addition, the features of these belts allow them to draw serpentine layouts around a high number of pulleys, thus avoiding the use of more than one belt. These belts have also improved reliability and fatigue life, while reducing wear, noise and vibrations. Serpentine V-ribbed belts can operate in both forward and backward directions and interact with ribbed or smooth pulleys.

The pulleys attached to the engine crankshaft and the alternator shaft are often in charge of filtering out the engine vibrations and their propagation to the alternator itself. In this category, one can find torsional vibration dampers, decoupling and isolation pulleys for the crankshaft side.[8] The alternator can also exploit overrunning dampers or pulleys to this end.[9,10]

In a serpentine BDS, the setting of a proper belt tension is of great importance. On the one hand, a high tension can cause premature failure of the bearings supporting the pulleys and of the belt itself. On the other hand, if the belt is too slack, excessive slip may occur. In this context, the belt tensioner has the role of maintaining a suitable amount of tension on the belt, especially on the slack span. The device is characterized by a small stiffness to guarantee the desired pretension over time, disregarding belt deformation or wear. The benefits of a tensioner on the dynamics of a BDS have been intensively investigated in previous works.[11–13]

When dealing with micro-hybrid systems, the tensioner features need to be extended to the operating conditions inherent to the use of a belt starter generator (BSG). The BSG represents the least invasive of the micro-hybrid technologies as it directly replaces the traditional alternator and requires only a larger and more performing battery.

In a conventional layout, the crankshaft pulley usually transmits part of the internal combustion engine (ICE) power to the belt while the other pulleys collect and transfer it to the accessories they are connected to. Hence, the belt tensioner is placed on one of the slack spans in order to maintain the tension inside a reasonable operating interval. In contrast with the traditional alternator, the BSG can be activated to work also as a motor, thus delivering power to the system. This mode changes the tensioning conditions of the BDS and leads to a fast exchange between slack and tight spans. Therefore, the traditional tensioner acting only on one span has a null effect on the system because the force associated to its low stiffness is easily overcome by the new tight span. As a result, the BSG-based BDS requires a dedicated tensioning mechanism able to quickly adapt itself to this dual tension behavior.

The operating conditions of the BDS are dictated by the working modes of the BSG: generator mode or motor mode. *Generator mode* is used to replicate the function of a traditional alternator that collects the power from the belt to charge the vehicle battery. Furthermore, it enables a regenerative braking function. *Motor mode* is exploited as an electric boost, where the BSG assists the ICE for transient accelerations. Moreover, this mode is also used for the start and stop function, through which the cranking of the ICE is performed without the need of a separate starter electric machine.

In Fig. 1, a BSG-equipped BDS is shown. It highlights the two belt spans that experience the alternation of tension when changing the operating condition. Each span needs to use a custom tensioning mechanism, indicated in Fig. 1 by the pulleys AT1 and AT2.

As previously stated, a traditional automatic tensioner is not sufficient to control the tension in both operating conditions of a BSG-based BDS. Solutions of different fashions have been adopted by manufacturers in the past: passive and active, one and two pulleys, linear and rotary. Some of these solutions are illustrated in Fig. 2.

According to their characteristics, it is possible to provide a classification of the existing tensioning solutions in BSG-based BDSs, as shown in Fig. 3. A first designation can

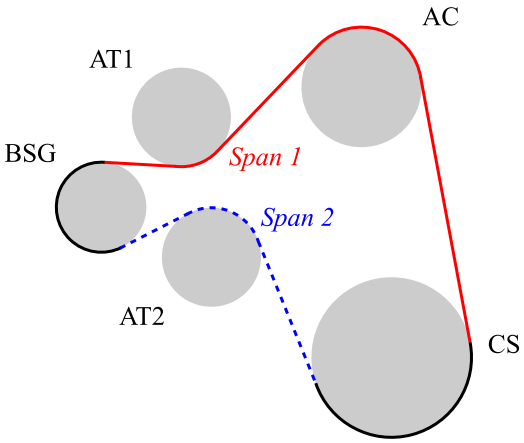

Figure 1. BDS layout mounting a BSG. The two belt spans are alternately tight and slack according to the operating mode of the BSG and require a dedicated tensioner (pulleys AT1 and AT2) to keep a suitable belt tension. The layout also presents crankshaft (CS) and air conditioning compressor (AC) pulleys.

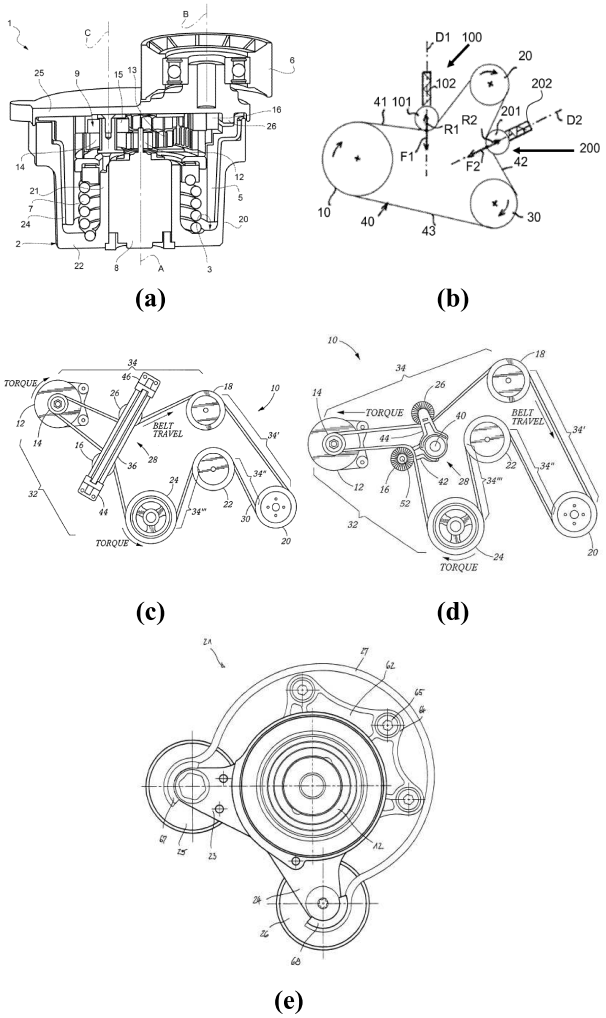

Figure 2. Different tensioning solutions for BSG Systems: (a) active tensioner by Dayco Europe S.r.l.;[14] (b) double tensioner by PSA Peugeot Citroen;[15] (c) linear tensioner by The Gates Corporation;[16] (d) Y tensioner by The Gates Corporation;[17] (e) rotary twin arm tensioner by Mubea Muhr und Bender KG.[18] The images were taken from the cited patents.

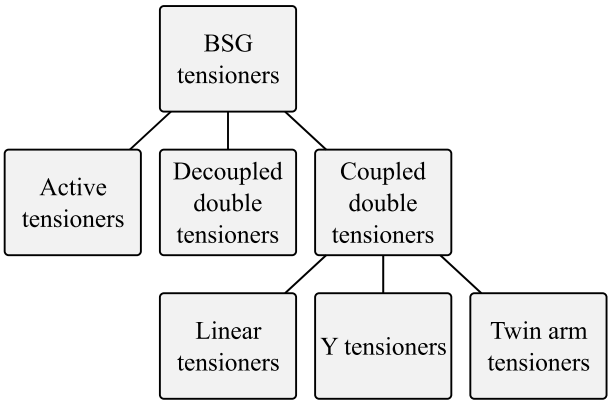

Figure 3. Classification of tensioning solutions for BSG-based systems.

be done between active tensioners and passive double tensioners. Active solutions consist of a single-pulley tensioner whose position is controlled by an actuator to adapt to the operating condition of the BDS. An example of this solution is the device proposed by Dayco Europe.[14] This active tensioner is characterized by an electric motor that moves the arm tensioner by means of a rotary gear stage. The main drawback of active tensioners is the need of a control and power stage to operate. In contrast, passive double tensioners are characterized by two pulleys whose operation can be independent or linked to each other. An example of decoupled double tensioners is provided by PSA Peugeot Citroen.[15] If required, the coupling between the two tensioner pulleys can be realized following different geometric patterns. The existing solutions offer linear, Y and rotary twin arm tensioners. The Gates Corporation provides good examples of linear[16] and Y tensioners.[17]

The (rotary) twin arm tensioner topology is the most used and investigated by important BDS component manufacturers, such as Dayco Europe, The Gates Corporation, Litens Automotive Partnership, Mubea Muhr und Bender KG and Schaeffler Technologies. Such diffusion can be mainly attributed to its constructive simplicity and passive feature.

Despite its popularity, the twin arm tensioner has been addressed almost exclusively by patents.[18–23] The number of research papers on this topic is still exiguous. The very few available research works regarding this device cover exclusively design and numerical simulation aspects.[24,25]

Thus, the state of the art lacks of experimental data able to demonstrate the benefits of the twin arm tensioner. In this context, the present paper focuses on the analysis of the performance of this device through experimental tests. These results are supported by a simplified static model able

to reproduce the fundamental behavior of the device and highlight its main functional features.

The remainder of this paper is organized as follows. First, it describes the static model of the twin arm tensioner. The model is subsequently used to reproduce the behavior of two BSG-based layouts equipped with twin arm and traditional tensioners, respectively. This task gives means for comparison between the two devices and highlights the benefits of the twin arm solution. Afterwards, the experimental setup and testing procedure are presented. Finally, the test results are discussed and compared to those obtained with the static model.

2 Twin arm tensioner

The twin arm tensioner considered in this work is a passive device composed by two pulleys connected by a torsional spring and rotating around a pivot that is coaxial relative to the BSG axis. Both tensioner pulleys move around the common pivot: this motion depends on the resulting hub loads and the spring torque of the tensioner.

The described system can lead to variations in the absolute position of the arms and their relative aperture. Furthermore, the hub loads on the two tensioner axes depend on the geometry of the system. Specifically, the pulley wrap angles define the arm forces and hence, the torque that arises around the tensioner pivot.

In this section, an analytical representation of the behavior of the tensioner is conducted by taking into account static equilibrium and geometry constraints. To this end, the following hypotheses must be adopted:

- The tensioner arms are considered infinitely rigid.
- The tensioner arms are considered perfectly hinged on their supports, where friction effects are neglected.
- The friction of the bearings of the pulleys is neglected.
- The tensioner spring acts with no friction and perpendicularly to the axis of each tensioner pulley.
- The belt does not dissipate energy.
- The belt is ideally rigid.

This last assumption holds for layouts equipped with a twin arm tensioner, where the effects of belt deformation are negligible when compared to those of the moving tensioner arms.

Figure 4 highlights the main variables and parameters to consider for the static analysis of the tensioner. The subsequent analytical description can be provided for both tensioner pulleys using the indexes $i = 1, 2$.

Following the initial assumptions, the torques acting on the tensioner pivot balance each other in static equilibrium,

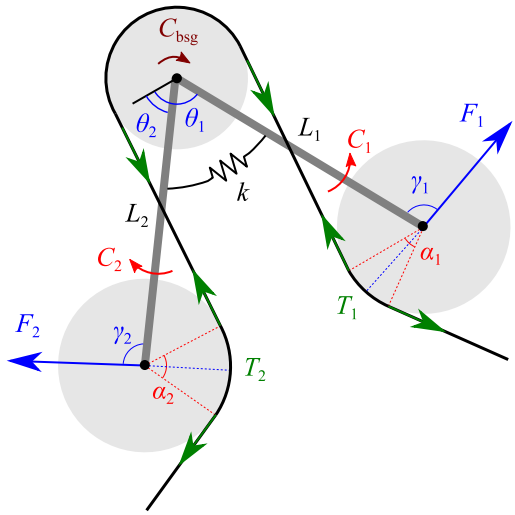

Figure 4. Scheme of the tensioner with variables and parameters of interest: belt tension T_i, arm force F_i, pulley wrap angle α_i, force angle γ_i, arm torque C_i, arm angle θ_i, arm length L_i, tensioner spring stiffness k, BSG torque C_{bsg}.

i.e.

$$C_1 = C_2, \tag{1}$$

and

$$C_i = F_i L_i \sin \gamma_i, \tag{2}$$

where F_i is the hub load measured on the pulley axis, L_i is the length of each tensioner arm and γ_i is the angle between the applied force and the corresponding lever arm.

Furthermore, the applied force on each arm depends on the tension of the belt span T_i and the wrap angle α_i:

$$F_i = 2T_i \sin\left(\frac{\alpha_i}{2}\right). \tag{3}$$

The established assumptions let the tensioner spring transmit the torque ideally from one arm to the other, and hence C_i is defined by the tensioner stiffness and relative displacement of the two tensioner pulleys:

$$C_i = k(\theta_v - \theta_u - \Delta\theta_0), \tag{4}$$

where k denotes the spring stiffness, $\Delta\theta_0$ is the angular aperture at null torque and θ_u and θ_v denote the angular displacement of the tensioner arms. The indexes u and v assume different values according to the operating mode:

- *Motor mode:* the BSG exerts electric traction.

$$\begin{cases} v & = 1 \\ u & = 2 \end{cases}$$

- *Generator mode:* the BSG functions as an alternator.

$$\begin{cases} v & = 2 \\ u & = 1 \end{cases}$$

Equations 1 to 4 emphasize the dependence between the angular position of the tensioner arms and the belt tension of both spans. In addition, the difference between the tensions of both belt spans is imposed by the BSG torque

$$C_{\mathrm{bsg}} = R_{\mathrm{bsg}}(T_v - T_u), \tag{5}$$

where R_{bsg} is the radius of the BSG pulley. If the BSG is not applying torque on the belt, the tensions T_u and T_v are equal to the pretension of the belt T_0. When the BSG acts on the system, $T_v > T_u$, where the indexes u and v are selected according to the working mode, as previously indicated.

To fully define the static model, the total length of the belt l_{tot} is constrained to its nominal value:

$$l_{\mathrm{tot}} = l_{\mathrm{nom}}. \tag{6}$$

The solution of the static model described through Eqs. 1 to 6 requires the full geometry of the transmission. Hence, the analytical formulation of contact points, wrap angles and belt span lengths is provided in the following.

In a serpentine belt drive system, the belt wraps around the pulleys in both forward and backward directions. Therefore, four configurations between the belt and adjacent pulleys are possible: two direct and two crossed (see Fig. 5). For each possible configuration, the contact points at the entry or exit of the pulley are described by

$$x_{p,ti} = x_i + R_i \cos(\xi_i \pm \beta_{tj}) \tag{7}$$

$$y_{p,ti} = y_i + R_i \sin(\xi_i \pm \beta_{tj}) \tag{8}$$

where x_i, y_i are the Cartesian coordinates of the pulley center and R_i is the pulley radius. The angle between the horizontal and the line connecting the centers of the ith and jth pulleys is indicated as ξ_i, while β_{tj} is the angle between the horizontal and the belt span itself. The index p indicates the nature of the contact point, whether it corresponds to the entry ($p = \mathrm{in}$) or the exit ($p = \mathrm{out}$) of the belt on the pulley. The index t indicates the belt span type, whether it is crossed ($t = \mathrm{c}$) or direct ($t = \mathrm{d}$).

Note that the position of a generic tensioner pulley with respect to the pivot point is dictated by the arm angle θ_i:

$$\begin{cases} x_i & = x_{\mathrm{bsg}} + L_i \cos\theta_i \\ y_i & = y_{\mathrm{bsg}} + L_i \sin\theta_i \end{cases}, \tag{9}$$

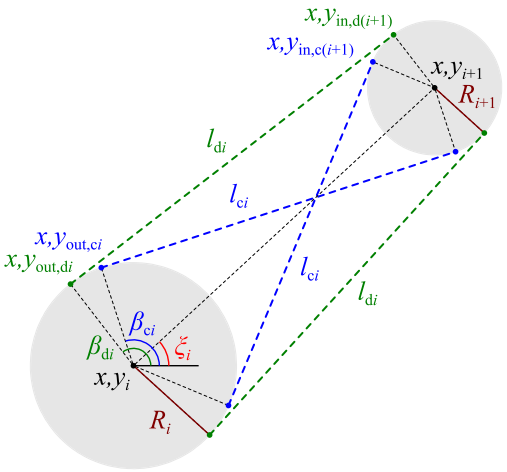

Figure 5. Geometry of the connection between two adjacent pulleys.

where, as previously described, the pivot of the tensioner arms is placed on the center of the BSG pulley $x_{\mathrm{bsg}}, y_{\mathrm{bsg}}$.

The length of the belt span is given by the distance between the exit contact point on the ith pulley and the entry contact point on the jth pulley:

$$l_{ti} = \sqrt{(x_{\mathrm{in},tj} - x_{\mathrm{out},ti})^2 + (y_{\mathrm{in},tj} - y_{\mathrm{out},ti})^2}. \tag{10}$$

Also, the wrap angle of the belt on the pulley can be defined as the angular distance between the entry and exit contact points.

$$\alpha_i = 2 \arcsin\left[\frac{\sqrt{(x_{\mathrm{out},ti} - x_{\mathrm{in},ti})^2 + (y_{\mathrm{out},ti} - y_{\mathrm{in},ti})^2}}{2R_i}\right]. \tag{11}$$

For a generic pulley of radius R_i, the wrap length is simply

$$l_{\mathrm{w}i} = R_i \alpha_i, \tag{12}$$

and hence, the total length of the belt is calculated as the sum of spans and wraps:

$$l_{\mathrm{tot}} = \sum_i l_{\mathrm{w}i} + l_{ti}. \tag{13}$$

Finally, the angle γ_i between the applied forces F_i and the corresponding lever arms L_i can be expressed as

$$\gamma_i = \pi - \frac{\alpha_i}{2} - \arccos\left(\frac{R_{\mathrm{bsg}} + R_i}{L_i}\right) \tag{14}$$

The obtained geometric expressions (Eqs. 7 to 14) can be substituted into the equations of the static model (Eqs. 1 to 6). For solving purposes, the resulting system of equations requires the geometric parameters (pulley radii R_i and

tensioner arm length L_i) and the level of belt pretension T_0. With these inputs, it is possible to calculate the initial position x_{0i}, y_{0i} for all the pulleys and the nominal belt length l_{nom}. Subsequently, a known BSG torque C_{bsg} is applied and the solution of the static model yields the tension of the belt spans T_i and the angle of the tensioner arms θ_i associated to the given load.

In practice, the equation set was implemented in MATLAB and solved using a trust-region dogleg nonlinear method.

2.1 Performance assessment

The solution of the described system of equations for a given BDS layout is shown in Fig. 6. The standstill layout ($C_{\mathrm{bsg}} = 0$) is compared to the one obtained with different BSG torque values: 10 and 30 Nm both in motor and generator modes. The plots show the direction of rotation of the crankshaft and the nature of the BSG torque. In motor mode, the BSG torque and the crankshaft speed present the same direction, whereas in generator mode, they are opposite.

Moreover, a variation in C_{bsg} produces a change in the absolute angle of both tensioner arms and the relative aperture among them. Fig. 6 also shows the dependence of the tensioner behavior on the geometry of the system. When the tensioner arms move, the wrap angles of the tensioner and the adjacent pulleys change. Consequently, the length and position of the belt spans are also modified.

Table 1 lists the performance data corresponding to each condition addressed in Fig. 6 for a pretension of $T_0 = 288$ N and a starting position of $\theta_1 = 75.7°$ and $\theta_2 = 141.7°$. The output data are the belt tension on both the tight and the slack spans, the wrap angle and the sliding arc on the BSG pulley. This latter quantity is defined according to Euler's formula

$$\phi_{\mathrm{s}} = \frac{1}{\mu_{\mathrm{r}}} \ln\left(\frac{T_v}{T_u}\right), \tag{15}$$

and the equivalent friction coefficient is given by

$$\mu_{\mathrm{r}} = \frac{\mu}{\sin(\delta/2)} = 1.2, \tag{16}$$

where μ is the static friction coefficient and δ is the pulley rib angle.

In Table 1, the sliding arc is indicated as a percentage of the wrap angle to better highlight its influence on the performance of the transmission.

Results demonstrate that a twin arm tensioner yields relative sliding arcs below 40% of the wrap angle for the calculated conditions. This means that a total slip situation is never reached, even with very high torque requests from the BSG. In addition, the tension of the slack span is kept at around 85% of the belt pretension; it stays well within a tension gap that guarantees a proper transmission efficiency and avoids excessive belt slip. It is worth mentioning that these outcomes are obtained for both motor and generator working modes.

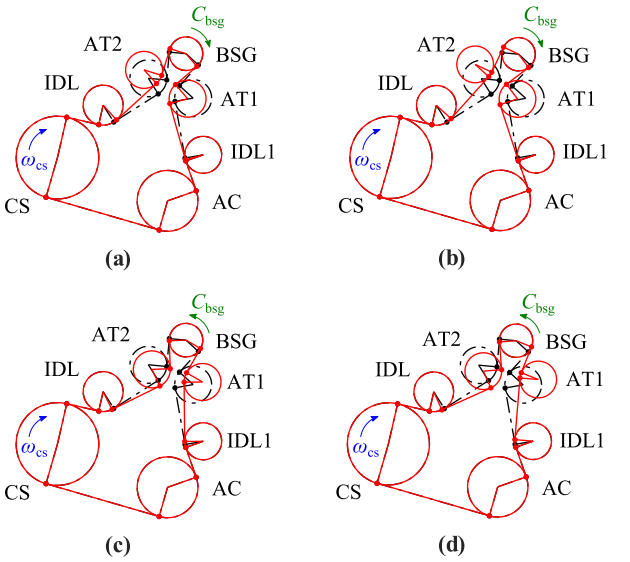

Figure 6. Geometry of a BSG-based BDS equipped with a twin arm tensioner for different operating conditions. Working geometries (solid) are compared with standstill (dashed). The BSG is driven at (a) 10 Nm and (b) 30 Nm in motor mode, and (c) -10 Nm and (b) -30 Nm in generator mode. The layout is constituted by crankshaft (CS), air conditioning compressor (AC), idlers (IDL and IDL1), tensioner pulleys (AT1 and AT2) and BSG. The directions of the crankshaft speed ω_{cs} and the BSG torque C_{bsg} are also indicated.

To highlight the advantages of the twin arm solution over a traditional tensioner, Fig. 7 shows the behavior of the same BDS equipped with this latter device. Here, the AT1 pulley is fixed, whilst AT2 acts as a single arm tensioner to guarantee proper tension of the slack span in generator mode. Additionally, the belt length constraint (Eq. 6) does not hold anymore because belt deformation is mandatory to allow the motion of the single-arm tensioner. To overcome this issue, the belt is assumed extensible inside a range of $\pm 0.7\%$ of its nominal length. A BSG torque of 10 Nm is then applied in both motor and generator modes. The corresponding performance data are reported in Table 2.

The performance drop in motor mode is evident with the traditional tensioner. The tension of the slack span dramatically decreases and the sliding arc results above 50% of the whole wrap angle. Moreover, it was not possible to obtain feasible results at $C_{\mathrm{bsg}} = 30$ Nm, as this case would lead to a total slip condition where the tensioner pulley and the belt loose contact. The obtained results indicate that

Table 1. Performance results of a BSG-based BDS system using a twin arm tensioner.

condition	BSG mode	BSG torque [Nm]	tight span tension [N]	slack span tension [N]	BSG sliding arc [%]	BSG wrap angle [deg]
(a)	motor	10	603.5	250.5	19.8	212
(b)	motor	30	1307.6	247.7	38.2	207.6
(c)	generator	−10	600.9	247.7	19.9	212
(d)	generator	−30	1317.7	257.8	37.8	206

Table 2. Performance results of a BSG-based BDS system using a traditional tensioner.

condition	BSG mode	BSG torque [Nm]	tight span tension [N]	slack span tension [N]	BSG sliding arc [%]	BSG wrap angle [deg]
(a)	motor	10	450.1	49.6	55	191.2
(b)	generator	−10	568.2	247.7	17.7	223.5

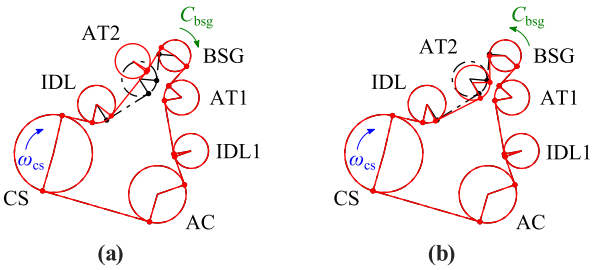

Figure 7. Geometry of a BSG-based BDS equipped with a traditional tensioner for different operating conditions. Working geometries (solid) are compared with standstill (dashed). The BSG is driven at (a) $10\ \mathrm{Nm}$ in motor mode and (b) $-10\ \mathrm{Nm}$ in generator mode. The layout is constituted by crankshaft (CS), air conditioning compressor (AC), idlers (IDL and IDL2), tensioner pulleys (AT1 and AT2) and BSG. The directions of the crankshaft speed ω_{cs} and the BSG torque C_{bsg} are also indicated.

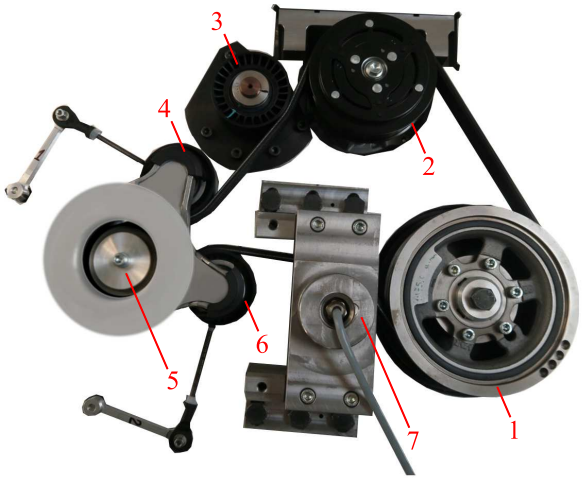

Figure 8. The investigated BDS layout features 7 pulleys: (1) crankshaft, (2) air conditioning compressor, (3,7) idlers, (4) tensioner arm AT1, (5) BSG, (6) tensioner arm AT2.

the traditional tensioner is inadequate to operate in BSG-equipped BDSs, mainly due to its inability to adapt to the exchange between tight and slack spans.

3 Experiments

3.1 Test rig

Experiments were conducted with a dedicated test rig in our laboratory. The system was designed with the aim of creating an environment able to reproduce the working conditions with good accuracy and repeatability. This goal motivated the choice of a full-electric configuration with two electric motors that replicate the behavior of the crankshaft and BSG pulleys. The use of electric drives offers improved repeatability and control of the output variables. It also reduces considerably the costs associated to the maintenance of a traditional engine test cell and allows to reproduce different layouts by suitably modifying or replacing the mechanical interface that supports the electric motors and the accessories.

Figure 8 shows the BDS layout used for experimental assessment. The transmission features seven pulleys: crankshaft, air conditioning compressor, two idlers, BSG and twin arm tensioner. For the purpose of this research, the air conditioning compressor is always kept in idle mode during the tests. Two Bosch Rexroth brushless motors from the IndraDyn H series replicate the behavior of the crankshaft and the BSG. Each machine is controlled by dedicated IndraDrive inverter. The crankshaft is a 38-kW motor with maximum speed and torque of $12\ \mathrm{krpm}$ and $320\ \mathrm{Nm}$, respectively. The BSG side is a smaller machine ($17\ \mathrm{kW}$) able to reach $22.5\ \mathrm{krpm}$ of speed and $45\ \mathrm{Nm}$ of torque. The complete selection process of the two electric motors can be found in our previous works.[26]

The test rig hosts different sensors to measure the transmission system variables during operation. The position feedback of both motors is accomplished with two Heidenhain ERM magnetic encoders (192 lines of resolution). The torques of the two motors are calculated from the corresponding current feedback values in the direct and quadrature axes. The angular positions of the tensioner arms are measured by means of two Kuebler KIS incremental

encoders (2500 lines of resolution). As seen in Fig. 8, each encoder is hinged to its respective tensioner pulley by means of a two-link kinematic arrangement. This mechanism is designed to follow and reproduce the angular displacement of the tensioner arms. The tension in both belt spans is measured on the two idler pulleys, which are equipped with Magtrol DB radial load cells (maximum force of 750 N). Their output is fed through an HBM Force Measurement System amplifier.

A dSpace MicroLabBox Platform is used to support a human-machine interface that commands the inverters and acquires the signals of interest. This system communicates with a host PC via Ethernet and with both motor inverters through CANOpen protocol. The inverters receive torque or speed reference values from the MicroLabBox device. In turn, they yield the actual measurements of speed and current of both motors. In the dSpace hardware, the 14-bit analog channels are used to read the load cell amplified signals, while the tensioner arm encoders are processed by direct capture inputs.

3.2 Procedure

The testing phase aims to verify the functionality of a twin arm tensioner installed on a BDS with a BSG device operating in motor and generator modes. In addition, experimental behaviors can be compared to the outputs of the static model. To simplify the analysis of the studied device, quasi-static tests were carried out.

Before the experiments, the belt pretension is set to 288 N. This force is verified with a CLAVIS type 6 belt tension meter. In each test, the crankshaft speed ω_{cs} is fixed to a constant value. Then, a torque ramp is applied with the BSG to load the system. The sign of this torque defines whether the BSG operates as a motor $(+)$ or as a generator $(-)$. A sufficiently low slope of ± 1 Nm/s is followed to avoid the introduction of unwanted inertial effects. When the system reaches the peak torque value $\hat{C}_{\mathrm{bsg}}$, the system is stopped. In this study, the tensioner arm angles and the belt span tensions are measured during the torque ramp of the BSG.

The following conditions were tested:

1. $\hat{C}_{\mathrm{bsg}} = +30$ Nm, $\omega_{\mathrm{cs}} = 860$ rpm, motor mode
2. $\hat{C}_{\mathrm{bsg}} = +30$ Nm, $\omega_{\mathrm{cs}} = 2500$ rpm, motor mode
3. $\hat{C}_{\mathrm{bsg}} = -30$ Nm, $\omega_{\mathrm{cs}} = 2500$ rpm, generator mode
4. $\hat{C}_{\mathrm{bsg}} = -17$ Nm, $\omega_{\mathrm{cs}} = 3800$ rpm, generator mode

The air conditioning compressor was kept idle in all the tests for the sake of simplicity.

In the first two conditions, the BSG boosts the BDS. In a vehicle, this boost feature is attractive at low engine regimes to deliver a short but fast acceleration. By converse, in the last two conditions, the BSG behaves as a generator that brakes the transmission. At high engine speeds, regenerative braking is desirable to recover part of the mechanical power in the front end accessory drive. Due to power limitations of the BSG machine, the test at 3800 rpm reaches a lower peak torque of -17 Nm.

The execution of the tests at different speeds is important to prove the validity of the static model, where the speed component and the friction effects associated to it are neglected.

Furthermore, the tests at mid speed (2500 rpm) span torque values in motor and generator modes. They are useful to highlight the dual behavior provided by the tensioner.

3.3 Results

Figure 9 shows the experimental results collected in the four described testing conditions. It exhibits the two tensioner arm angular displacements relative to their position at rest, the span tensions and the BSG sliding arc relative to its wrap angle. Furthermore, the data from the static model are also presented. These numerical results are obtained by solving the model with BSG torque values ranging from -30 to 30 Nm. The sliding arc on the BSG pulley is calculated for both numerical and experimental cases according to Eq. 15.

Numerical and experimental results highlight the behavior of the twin arm tensioner, which is capable to obtain comparable performances in both generator and motor modes.

In motor mode, the belt span on the pulley AT2 exhibits a tension directly proportional to the BSG torque. As this torque increases, it is seen that both arm angles tend to rotate in a negative (clockwise) direction. The arm with the pulley AT2 follows a larger displacement, thus yielding the aperture of the tensioner and a deflection of its spring. Additionally, the tension of the belt span facing the pulley AT2 has a linear increase with respect to the motor torque. In contrast the tension of the AT1 side stays within 80% of the pretension value.

In generator mode, a similar behavior occurs, but the roles of AT1 and AT2 are inverted. Both arms rotate counterclockwise and an aperture of the tensioner is still advisable as the braking torque increases.

As expected from Euler's formula (Eq. 15), the sliding arc is symmetric with respect to the ordinate axis. The maximum observed sliding arc assumes a value of 40.5%. Hence, the system works in a stable slip-safe condition.

The experimental results at different speeds are very close to each other in both modes. However, during the tests, it

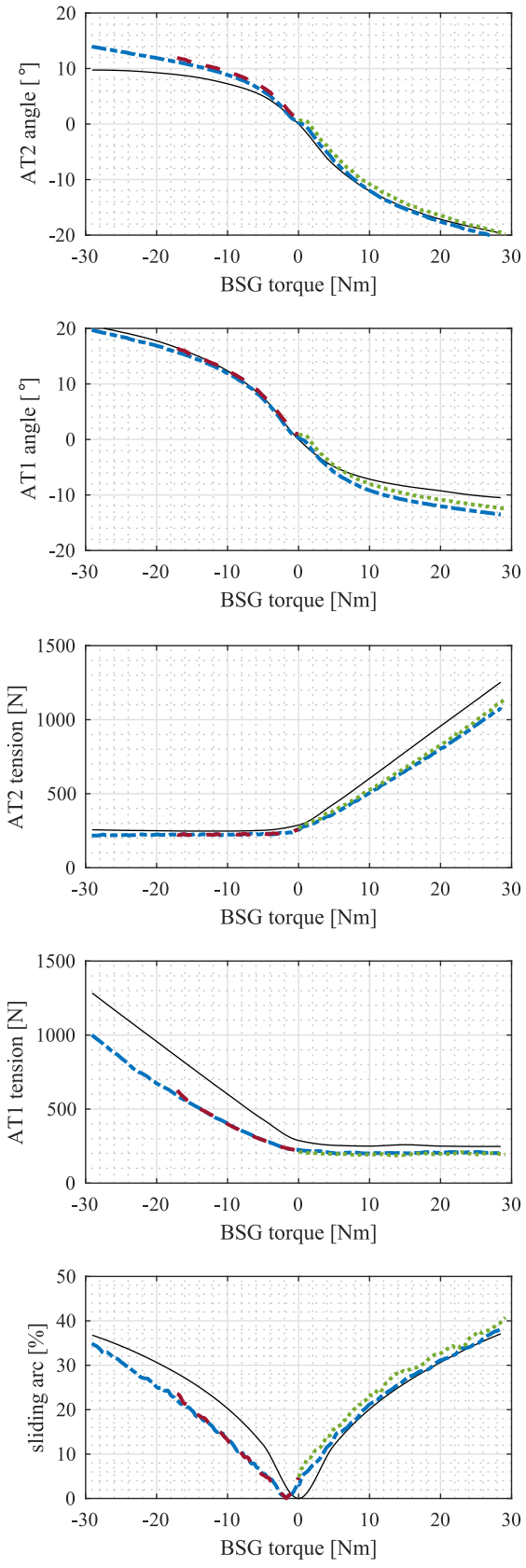

Figure 9. Results of a twin arm tensioning device working on a BSG-based BDS in motor and generator modes. The considered variables are the angular displacement of the tensioner pulleys, the belt span tensions and the sliding arc on the BSG pulley. Numerical results (solid) are compared to experimental data obtained at 860 rpm (dot), 2500 rpm (dash-dot) and 3800 rpm (dash).

was observed that the BSG required a torque between 1.5 and 2 Nm in motor mode to overcome the mechanical losses of the transmission. While this value counteracts the BSG in motor mode, it yields a braking contribution in generator mode. As a result, the measurements are shifted towards negative values of BSG torque by the indicated amount.

Some considerations must be made to better understand possible discrepancies between numerical and experimental results. The measurement of the belt tensions is indirect, as it goes through the measurement of the hub loads exerted by the belt on the shafts of the two idler pulleys. The belt tension is then calculated by the inverse of Eq. 3. Therefore, it is inversely proportional to the sine of half the idler wrap angle: small angles will inevitably lead to large measurement errors. This situation is particularly advisable for the idler on the AT1 pulley side. Furthermore, during the setup of the test bench, the load cell measurement axis is prone to misalignment with respect to its nominal angular position, thus inducing further errors in the tension estimation.

All in all, numerical and experimental results show an acceptable agreement that is sufficient to confirm the functional validity of the twin arm tensioner.

4 Conclusions

In this paper the performances of a twin arm tensioning device were highlighted. As a first step, a static model was used to show the functioning principles of the tensioner and its dependence on the geometry of a BSG-based transmission. The twin arm tensioner was then numerically compared to a traditional single-arm tensioner by studying their performance in motor and generator BSG modes. Afterwards, experiments were carried out to analyze the behavior of the twin arm tensioner. This experimental phase confirmed the favorable features of twin arm tensioning device in a BSG-based BDS layout. Furthermore, they proved that the proposed model can reproduce the behavior of the tensioner in quasi-static conditions.

Declaration of conflicting interests

The authors declare that there is no conflict of interests.

References

1. Gerbert GG. Paper XII (i) On Flat Belt Slip. In: Dowson D, Taylor CM and Godet M (eds) *Tribology Series vol. 18: Vehicle Tribology*. Elsevier, 1991, pp.333-340.
2. Gerbert G. Belt Slip–A Unified Approach. *J Mech Des* 1996, 118(3):432-438.

3. Tonoli A, Amati N and Zenerino E. Dynamic Modeling of Belt Drive Systems: Effects of the Shear Deformations. *J Vib Acoust* 2006, 128(5):555-567.
4. Gerbert BG. Power Loss and Optimum Tensioning of V-Belt Drives. *J Eng Ind* 1974, 96(3):877-885.
5. Chen TF, Lee DW and Sung CK. An experimental study on transmission efficiency of a rubber V-belt CVT. *Mech Mach Theory* 1998, 33(4):351-363.
6. Balta B, Sonmez FO and Cengiz A. Experimental identification of the torque losses in V-ribbed belt drives using the response surface method. *Proc IMechE Part D: J Automobile Eng* 2015, 229(8):1070-1082.
7. Hansson H. Geometry Conditions for Good Power Capacity in a V-Ribbed Belt Drive. *J Mech Des* 1990, 112(3):437-441.
8. Shangguan W-B and Feng X. Design of Isolation Pulley in Front of Crankshaft to Reduce Vibrations of Front End Accessory Drive System. SAE paper 2015-01-2254, 2015.
9. Xu J and Antchak J. New Technology to Improve the Performance of Front End Accessory Drive System. SAE paper 2004-01-3017, 2004.
10. Zeng X and Shangguan W-B. Modelling and optimisation dynamic performances for an engine front end accessory drive system with overrunning alternator decoupler. *International Journal of Vehicle Noise and Vibration* 2012, 8(3):261-274.
11. Ulsoy AG, Whitesell JE and Hooven MD. Design of Belt-Tensioner Systems for Dynamic Stability. *J Vib, Acoust, Stress, and Reliab* 1985, 107(3):282-290.
12. Hwang S-J, Perkins NC, Ulsoy AG et al. Rotational Response and Slip Prediction of Serpentine Belt Drive Systems. *J Vib Acoust* 1994, 116(1):71-78.
13. Leamy MJ and Perkins NC. Nonlinear Periodic Response of Engine Accessory Drives With Dry Friction Tensioners. *J Vib Acoust* 1998, 120(4):909-916.
14. Cariccia G, Licata FD and Noe E. *Actuated tensioner for an accessory drive*. Patent EP2864609 A1, Italy, 2015.
15. Pitaud B. *Systeme de mise sous tension dune courroie*. Patent FR2956889 B1, France, 2010.
16. Serkh A. *Dual linear belt tensioner*. Patent US7419447 B2, USA, 2008.
17. Ali I, Liu K and Hanes D. *Accessory and motor/generator belt drive tensioner*. Patent CA2424256 C, USA, 2007.
18. Jud J and Jung MD-I. *Riemenspannvorrichtung fr Starter-Generator-Anwendung Belt tensioner for starter generator application*. Patent DE102008025552 A1, Germany, 2009.
19. Di Giacomo T and Lemberger H. *Two-arm belt tensioner*. Patent US20070037648 A1, USA, 2007.
20. Wolf B and Arneth R. *Belt tensioner*. Patent US20140256488 A1, Germany, 2014.
21. Harvey J, Stegelmann O, Martinez A et al. *Orbital Tensioner*. Patent WO2015167602, USA, 2015.
22. Antchak JR, Ryeland GW and Farewell R. *Endless drive arrangement for hybrid vehicle using two-armed tensioner with non-orbiting arms*. Patent WO2016123723 A1, Canada, 2016.
23. Deneszczuk WC and Maguire JM. *Drive belt tensioner for motor generator unit*. Patent US8602930 B2, USA, 2013.
24. Olatunde A and Zu JW. Optimization of Twin Tensioner Performance in a Belt-Driven Integrated Starter-Generator System for Micro-Hybrids. In: *ASME 2009 International Design Engineering Technical Conferences and Computers and Information in Engineering Conference*, San Diego, CA, USA, August 30-September 2 2009, paper no. DETC2009-87110, pp.951-957. New York: ASME.
25. Olatunde AO. *Design and Analysis of a Tensioner for a Belt-driven Integrated Starter-generator System of Micro-hybrid Vehicles*. PhD thesis, University of Toronto, Canada, 2009.
26. di Napoli M, Straehle M, Ruzimov S et al. Intelligent Belt Drive Systems in Hybrid Powertrains: a Multipurpose Test Rig. *IFAC-PapersOnLine* 2016, 49(21):47-53.